International Symposium
On Turbulence and Shear Flow
Phenomena (TSFP-9)
June 30 - July 3, 2015 *Melbourne, Australia*

Wall scaling laws for high-Reynolds-number turbulent pipe flow at $Re_\tau = 3008$

Junsun Ahn
Dept. of Mechanical Engineering
KAIST
Daejeon 305-701, Korea
junsun_ahn@kaist.ac.kr

Jae Hwa Lee
Dept. of Mechanical and Nuclear Engineering
UNIST
Ulsan 689-798, Korea
jhlee06@unist.ac.kr

Jin Lee
Dept. of Mechanical Engineering
KAIST
Daejeon 305-701, Korea
jin_lee@jhu.edu

Hyung Jin Sung
Dept. of Mechanical Engineering
KAIST
Daejeon 305-701, Korea
hjsung@kaist.ac.kr

ABSTRACT

A direct numerical simulation of turbulent pipe flow is performed at Re_τ = 3008 with a long streamwise domain length (30R) to investigate wall scaling laws in the physical and wavenumber spaces. The power law follows the streamwise mean velocity in the overlap region, y^+ = 90 – 300, evaluated by the power law indicator function. The scale-separated Reynolds shear stress shows that the large-scale motions ($\lambda_x^+ > 3000$) are more responsible to construct the constant-stress layer than the small-scale motions ($\lambda_x^+ < 3000$), and thus it is proposed that the large-scale motions more contribute to the growth of the mean velocity in the overlap region than the small-scale motions. In the pre-multiplied energy spectra of the streamwise velocity fluctuations, the k_x^{-1} region ssociates with the attached eddies appeared in λ_x/R = 2 – 5 at y^+ = 90 – 300 with the bimodal distribution. Linear growth of small-scale energies to large-scale energies helps to appear the k_x^{-1} region at high Reynolds number.

INTRODUCTION

Scientific technical advancements have enabled us to reliably measure flow velocity profiles at high Reynolds numbers of up to $Re_\tau \approx 10^5$ in experimental turbulent pipe flows (Hultmark et al. 2013). Many direct numerical simulations (DNSs) of turbulent pipe flows have been performed, although the Reynolds numbers in these simulations have been limited to $Re_\tau = O(10^3)$ due to the massive computational power and cost. The previous highest Reynolds number in DNS of turbulent pipe flow was Re_τ = 2003 in short streamwise domain length (Chin et al. 2014a). Since a streamwise domain length is an important parameter to capture very-long meandering structures without the distortion of high-order statistics, the DNS of the high Reynolds number with the long enough streamwise domain is demanding significantly.

Recently the streamwise mean velocity (U), which is the most fundamental quantity, has been newly focused on many researchers (e.g. Marusic et al. 2013). However the validation of the mean velocity is limited to the spatial resolutions of flow fields, because the indicator functions of the mean velocity are determined by the spatial derivatives along the wall-normal direction. It is known that there is the overlap region, where the inner and outer scalings are simultaneously satisfied. The inner scaling variables are the friction velocity (u_τ) and the viscous length scale (ν/u_τ), where ν is the fluid kinematic viscosity. The outer scaling variables are the flow thickness, but the appropriate velocity scale is the same as that used in the inner region. These two scales lead to the most famous logarithmic law (log law) in the overlap region, $U^+ = \kappa^{-1}\log(y^+) + B$, where κ is the von Kármán constant, B is the additive constant, y is the wall-normal distance, and the superscript + indicates the inner scaling. Most experimental and numerical studies of wall-bounded turbulent flows have documented the log law over a wide range of Reynolds numbers (Monty et al. 2009; Marusic et al. 2013); however, turbulent pipe flows do not always follow the log law in the mean velocity. Wu & Moin (2008) showed the power law in the mean velocity (Re_τ = 1142), defined as $U^+ = C(y^+)^\gamma$, where C is the proportional constant and γ is the power constant. Chin et al. (2014a) reported that the log law did not exist up to Re_τ = 2003. In experiments ($Re_\tau > 5000$), McKeon et al. (2004) observed both the power and log laws, depending on y^+: the power law was observed over $50 < y^+ < 300$ and the log law was observed over $600 < y^+ < 0.12Re_\tau$. However, experimental studies have revealed that the log law applies in pipe flow as well as channel flow at Re_τ = 1000 – 3000 (Monty et al. 2009). Note that at extremely high Reynolds numbers, the mean velocity in turbulent pipe flow was found to naturally converge to the log law (Hultmark et al. 2013). These distinct laws that conflicted in the overlap region motivate us to simulate a high-Reynolds-number turbulent pipe flow in the present study.

As the Reynolds number is increased up to $Re_\tau \approx 2000$, the outer regions of the pre-multiplied streamwise energy spectra of the streamwise velocity fluctuations ($k_x\Phi_{uu}{}^+$) become prominent (Hutchins & Marusic 2007). Kim & Adrian (1999) first observed the existence of very-large-scale motions (VLSMs) based on the bimodal distributions in the energy spectra. Rosenberg et al. (2013) observed traces of short and long wavelength peaks in turbulent pipe flows over a range of Reynolds numbers. Note that the presence of the long wavelength peak in the experimental studies, however, has been suspected to correspond to the

artifact of Taylor`s hypothesis (del Álamo & Jiménez 2009). In the energy spectra of high Reynolds number, furthermore, show the k_x^{-1} region, which is attributed to the attached eddy hypothesis (Perry et al. 1986). Nickels et al. (2005) and Rosenberg et al. (2013) respectively observed the k_x^{-1} region in turbulent boundary layer (TBL) at Re_τ = 14380 and turbulent pipe flow at Re_τ = 3334; however, Morrison et al. (2002) could not identify the k_x^{-1} region in the turbulent pipe flows at Re_τ = 1500 and 100000. Those features in the energy spectra are necessary to be confirmed by DNS without any assumption or logical contradiction.

The present study examines the DNS of a turbulent pipe flow at Re_τ = 3008, which becomes the highest Reynolds number in DNS of turbulent pipe flow, to explore the issues raised among high-Reynolds-number turbulent flows. The axial domain length is 30R, which is long enough to capture the large- and very-large-scale motions (LSMs and VLSMs). The streamwise mean velocity in the overlap region is observed with the power law based on the indicator function. The contributions of the LSMs and the small-scale motions (SSMs) on the Reynolds shear stress and the mean velocity are evaluated. In addition, the pre-multiplied streamwise energy spectra of the streamwise velocity fluctuations are examined with the bimodal distribution and the k_x^{-1} region with different-scaled turbulent structures.

NUMERICAL METHOD

The Navier-Stokes and continuity equations in cylindrical coordinates are employed to describe an incompressible and fully developed turbulent pipe flow 30R in length. The centerline velocity (U_c) and the pipe radius (R) are used to non-dimensionalize the equations. The governing equations are temporally discretized using the Crank-Nicolson scheme and are spatially resolved using the second-order central difference scheme with a staggered grid. The velocity and pressure are decoupled using the fully implicit fractional step method (Kim et al. 2002). No-slip conditions at the wall and periodic boundary conditions along the streamwise and azimuthal directions are employed. For convenience and for comparison with other geometries, the cylindrical coordinates are transformed to Cartesian coordinates (Monty et al. 2009). The time- and spatial-averaged quantities of the mean velocity and the velocity fluctuations are expressed using a capital letter or bracket (e.g., U or $\langle u' \rangle$). A detailed description of the numerical simulation can be found in Ahn et al. (2013).

The Reynolds number, calculated based on the pipe diameter (D) and the bulk velocity (U_b), is Re_D ($\equiv DU_b/\nu$) = 133000, and the Kármán number is Re_τ = 3008. The statistics are averaged over sampling times of $600R/U_c$, which allows a particle to travel 10 times down the axial domain length with the bulk velocity flow. A total of 12289 × 901 × 3073 grid points are employed, yielding a resolution in physical space of $\Delta x^+ = 7.34$ and $\Delta z^+ = 6.15$. A resolution along the wall-normal direction is $\Delta y^+_{min} = 0.36$ and $\Delta y^+_{max} = 9.91$. For the stable simulation, temporal resolution $\Delta t U_c/R = 0.003$ is adopted. A hybrid technique, a combination of OpenMP (Open Multi-Processing) and MPI (Message Passing Interface), is introduced to enhance the computational performance and to handle the massive memory. The simulations are performed using 4906 parallel cores (Intel Xeon X5570 2.93GHz) in the KISTI Supercomputing Center.

Figure 1 shows the numerical and experimental profiles of the streamwise mean velocity and the streamwise Reynolds stress in the turbulent pipe flows for validating the present results. The DNS data at Re_τ = 1142 (Wu & Moin 2008) and the experimental data at $Re_\tau \approx 3000$ (Monty et al. 2009) are included. The present mean velocity profile shows a similar trend with other data. The profiles of the streamwise Reynolds stress are in good agreement with that of Wu & Moin (2008) near the wall, and the difference along the wall-normal direction are shown due to the high Reynolds number. However, the experimental streamwise Reynolds stress (Monty et al. 2009) is scattered near the wall. Although the hot-wire resolution ($l^+ = lu_\tau/\nu$, where l is the hot-wire length) is small as $l^+ = 30$, it is possible to produce an attenuation of the small-scale structures (Chin et al. 2011).

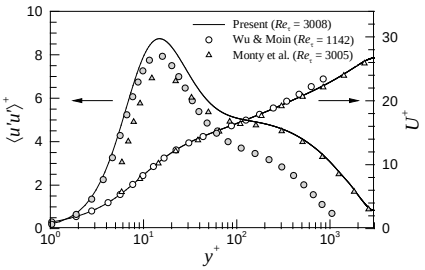

Figure 1: Profiles of the streamwise mean velocity and the streamwise Reynolds stresses. The hollow and solid symbols indicate the streamwise mean velocity and the streamwise Reynolds stress, respectively.

STREAMWISE MEAN VELOCITY

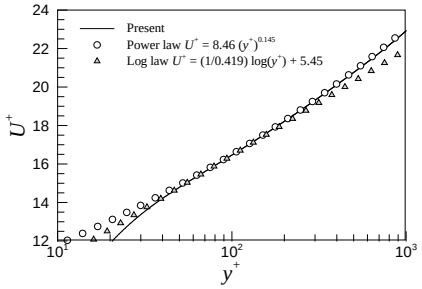

Figure 2: The streamwise mean velocity with the power and log laws.

The streamwise mean velocity is magnified along the buffer and overlap regions y^+ = 10 – 1000 in figure 2 with the power and log laws:

$$\text{Power law: } U^+ = C\left(y^+\right)^\gamma, \tag{1}$$

$$\text{Log law: } U^+ = \kappa^{-1}\log\left(y^+\right) + B. \tag{2}$$

The power law well follows the present mean velocity in the range of y^+ = 60 – 600 (y/R = 0.02 – 0.2), whereas the

log law matches the mean velociy only over the short range of $y^+ = 40 – 150$ (y/R = 0.013 – 0.05), both within a 0.5% tolerance. The coefficients of each law are obtained from the indicator functions in figure 3. Note that according to the suggestion of Marusic et al. (2013), the log region is predicted as $164 < y^+ < 451$ ($3(Re_\tau)^{1/2} < y^+ < 0.15Re_\tau$) for the present Reynolds number; however it locates higher than the present log region due to the higher Reynolds numbers employed in their experimental study. The present power law coefficients (C = 8.46, $\gamma = 0.145$) are almost the same as those ($C = 8.48$, $\gamma = 0.142$ at $Re_\tau > 5000$) reported by McKeon et al. (2004), indicating that the coefficients are independent of the Reynolds numbers. The satisfaction of the power law implies that the viscous effects of the wall remained in the overlap region (Barenblett 1993). Therefore, the power law behavior in the present pipe flow at $Re_\tau = 3008$ could be interpreted as the widely spread viscous effect along the wall-normal direction.

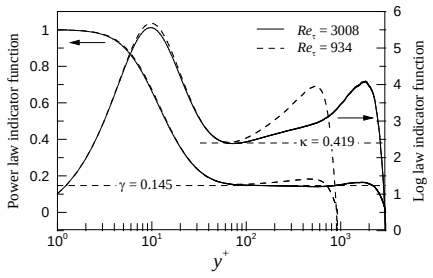

Figure 3: The power law and log law indicator functions.

Suitability of the power and log laws is evaluated by each indicator function according to:

$$\text{Power law indicator function}: \frac{y^+}{U^+}\frac{\partial U^+}{\partial y^+} = \gamma, \qquad (3)$$

$$\text{Log law indicator function}: y^+\frac{\partial U^+}{\partial y^+} = \frac{1}{\kappa}. \qquad (4)$$

The indicator functions are alternative forms of the mean velocity to show the satisfaction of each law. The indicator function implies that if a law is satisfied in a specific region, then there apears a constant in that region. Figure 3 shows the profiles of the indicator functions, including the DNS data obtained at $Re_\tau = 934$ (Ahn et al. 2013) for comparison of Reynolds numbers. The profiles of the power law indictor function at two Reynolds numbers collapse up to $y^+ \approx 100$. As increasing the Reynolds number, the profiles descend in the overlap region, and finally the curve corresponding to $Re_\tau = 3008$ reaches a plateau ($\gamma = 0.145$) over the range $y^+ \approx 90 – 300$ (y/R = 0.1). The profiles of the log law indicator function exhibit qualitatively consistent behaviors up to $y^+ \approx 60$ with a local minimum of 2.387 (= $1/\kappa$, $\kappa = 0.419$), which is very similar to 0.421 ± 0.002 found by McKeon et al. (2004). Note that the power and log regions from the indicator functions are more accurate than the observed regions in figure 2(b) because the effects of the plateau region or local minimum in the indicator functions make the visible wall-normal regions be stretched. Unlike the power law indicator function, no flat region but only local minimum region is observed in the log law indicator function. The absence of a flat region has been observed in previous DNS studies up to $Re_\tau \approx 2000$ (Wu & Moin 2008; Ahn et al. 2013; Chin et al. 2014a). McKeon et al. (2004) stated that a log law emerged as the Reynolds number increased ($Re_\tau > 5000$) although they did not examine the log law indicator function. The present investigation of the indicator functions, therefore, provides clear evidence that the present mean velocity follows the power law in the overlap region at the present Reynolds number ($Re_\tau = 3008$). Note that previous numerical and experimental studies of turbulent channel flows at $Re_\tau \approx 900 – 3000$ suggested the universal log law in the mean velocity, although a clear plateau was not observed in the log law indicator function (Hoyas & Jiménez 2006; Monty et al. 2009).

SCALE SEPARATION

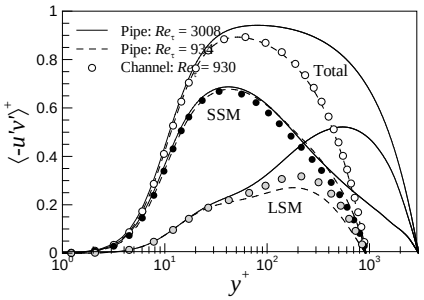

Figure 4: Scale-separated Reynolds shear strss of turbulent pipe flows at $Re_\tau = 3008$ and 934 and turbulent channel flow at $Re_\tau = 930$.

Absence of the log law is coincident to lack of the constant-stress layer, which continues the presence of the power law. Townsend (1976) derived the log law based on a constant-stress layer under the assumption of an infinite Reynolds number. The constant-stress layer indicates that the Reynolds shear stress is nearly independent of the distance from the wall. Although the present Reynolds number $Re_\tau = 3008$ is not infinitely high, it is meaningful to investigate the scale-dependent influences on the Reynolds shear stress by using wavelength decomposition. To demarcate the LSMs and SSMs, a cutoff wavelength $\lambda_x{}^+ = 3000$, where λ_x is a streamwise wavelength, proposed by Chin et al. (2014b), is employed. Here, the LSMs encompass the VLSMs, i.e., LSMs = LSMs + VLSMs. The same procedure to Chin et al. (2014b) is applied to the DNS data of pipe flow at $Re_\tau = 934$ (Ahn et al. 2013) and 3008, as shown in figure 4. It shows that the profiles of the SSMs are similar regardless of the Reynolds numbers, implying that the employed cutoff wavelength is appropriate. On the other hand, the LSMs increase in the outer region with increasing the Reynolds numbers. This suggests that in total Reynolds shear stress, the LSMs are more responsible to maintain the constant stress in the overlap region than the SSMs. Note that the wall-normal range of 1% tolerance of the maximum Reynolds shear stress (0.94165) is distributed along $y^+ = 50 – 140$, which is similar to the log region found in figure 2. We, therefore, conjecture that if the Reynolds number are increased further, the LSMs becomes more enhanced and the constant-stress layer would appear.

The geomeric difference of the scale-separated Reynolds shear stress is examined with the pipe and channel flows at $Re_\tau \approx 930$ (Ahn et al. 2013; Lee et al. 2014) in figure 4. The magnitude of the Reynolds shear stress associated with the LSMs in the overlap and core regions of the pipe flow is smaller than the magnitude in the channel flow ($y^+ \geq 50$). The contribution of the LSMs to the Reynolds shear stress is larger in the channel flow than in the pipe flow, even though the total Reynolds shear stresses are nearly equivalent. Note that the contributions of the SSMs in the outer region differ from the contributions of the LSMs toward the total Reynolds shear stresses in both flows. These different statistical behaviors of the LSMs come from the different geometries, which might determine the development speed of the mean velocity.

The structural differences between the pipe and channel flows probably result in different power and log laws that apply in the overlap region. Because the LSMs in the pipe flow decays more rapidly than in the channel flow due to space limitations in the core region, the LSMs in the pipe flow are more restricted to be developed than those in the channel flow. Lee et al. (2015) found that the survival time of the LSMs was shorter in the pipe flow than in the channel flow. Because the LSMs are more highly populated in the channel flow than in the pipe flow (Lee et al. 2015), the highly active LSMs in the channel flow contribute to the log law in the mean velocity with a greater extent than they did in the pipe flow.

ENERGY SPECTRA

Figure 5 shows the one-dimensional (1-D) pre-multiplied streamwise spectra of the streamwise velocity fluctuations in $y/R \leq 0.1$ along the outer coordinate. The profiles at $y^+ = 90 - 300$ agree well over the wavelengths $\lambda_x/R = 2 - 5$, creating a plateau. Note that these wavelength ranges are in accordance with $\lambda_x/y = 18 - 160$, expressed by the inner coordinate. For example, the curve at $y^+ = 90$ induces a plateau for $\lambda_x/y = 70 - 160$, and the curve at $y^+ = 300$ induces a plateau for $\lambda_x/y = 18 - 50$. These flat regions are called the k_x^{-1} region, where k_x is a wavenumber (Perry et al. 1986). Nickels et al. (2005) and Rosenberg et al. (2013) oberved the k_x^{-1} region in TBL ($Re_\tau = 14380$) and turbulent pipe flow ($Re_\tau = 3334$) at $y^+ \geq 100$. It is remarkable to note that in turbulent pipe flow at higher Reynolds numbers, Rosenberg et al. (2013) did not found the k_x^{-1} region, and instead the logarithmic correction of the k_x^{-1} region was observed; however since the nearest wall-normal location for the measurement was $y^+ \approx 400$, the k_x^{-1} region would appear at $y^+ \approx 100$.

The existence of the k_x^{-1} region supports the attached eddy hypothesis (Perry et al. 1986). Attached eddies are energy-containing motions and are proportional in size to the distance between their centers and the wall, i.e., attached to the wall (Townsend 1976). Nickels et al. (2007) revealed that the log law did not readily describe the mean velocity without employing the attached eddy hypothesis. Similarities, therefore, could be achieved by satisfying both the k_x^{-1} region and the log law. A state, in which both the k_x^{-1} region in the wavenumber space and the log law in the physical space are satisfied, is termed complete similarity, free from viscous effects (Townsend 1976). The beginning and ending locations of the k_x^{-1} region, $y^+ = 90$ and 300, however, are almost equivalent to the power region from the power law indicator function in figure 3, which implies incomplete similarity (Morrison et al. 2002). Because the mean velocity follows the power law, the viscous effects persist in the physical overlap region, although the k_x^{-1} region appears without the viscous effects in the spectra. Note that it is widely accepted that the log law is satisfied with extremely high Reynolds numbers. In this reason, it is proposed that as increasing Reynolds numbers, the similarity is firstly achieved in the wavenumber space with the k_x^{-1} region and then satisfies with the log law in the physical domain.

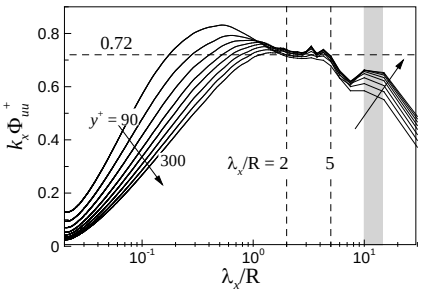

Figure 5: 1-D pre-multiplied streamwise spectra of the streamwise velocity fluctuations at $y^+ = 90 - 300$ with the interval of $\Delta y^+ = 30$ along the outer coordinate. The grey band represents the wavelength range $10 < \lambda_x/R < 15$.

Another interesting observation of the bimodal distributions is shown in figure 5. There are clear two peaks of the SSMs or LSMs and the VLSMs. The short wavelength spectral peaks of the SSMs or LSMs grow with increasing the wall-normal distance up to $\lambda_x/R = 3$. A long wavelength spectral peaks of the VLSMs are observed for $\lambda_x/R = 10 - 15$, depicted by the grey band. Note that because the grid system employed here permits the streamwise wavelengths up to $30/n$ (n is an integer between 1 and $N_x/2$, where N_x is the number of the grid along the streamwise direction), the wavelengths of the VLSMs are only 15R, 10R, and so on, creating large variations in the long wavelengths shown in figure 6. Even though there are discrete gaps in long wavelengths, the overall spectral shapes, however, are not affected. The long wavelength spectral peak does not surpass the peak at short wavelength spectra peak. It is different from other experimental results (e.g. Monty et al. 2009), which comes from the overestimated energy of the VLSMs due to the usage of Taylor`s hypothesis (del Álamo & Jiménez 2009). The long wavelength energy at $\lambda_x/R = 10 - 15$ increases as the wall-normal distance increases although there is a deep valley at $\lambda_x/R = 7.5$. It seems that the deep valley passively occurs due to the sudden increase associated with the energy of the VLSMs. This sudden energy increase at long wavelengths is not observed in the low-Reynolds number pipe flows (Ahn et al. 2013; Chin et al. 2014a).

Figure 6 shows a two-dimensional (2-D) contour map of $k_x\Phi_{uu}^+$. There is an obvious inner site at $y^+ = 13$ with $\lambda_x^+ = 800$ due to the self-sustaining near-wall cycle (Hutchins & Marusic 2007). In the overlap region, an outer site is also shown at $y/R = 0.087$ with $\lambda_x/R = 10$, which has been firstly

observed in the DNS of turbulent pipe flow. The presence of an outer site has been reported in many experiments as resulting from the activation of VLSMs (Hutchins & Marusic 2007; Monty et al. 2009; Rosenberg et al. 2013). The short wavelength spectral peaks along the wall-normal location are detected in the 1-D energy profiles, and they compose of the linear trend, λ_x/R = 20y/R (white dashed line). The small-scale energies near the wall grow into the outer-layer large-scale energies followed by the linear fashion. The linear growth of the structures is closely associated with the k_x^{-1} region denoted by the black solid box (λ_x/R = 2 – 5 with y^+ = 90 – 300). At low Reynolds numbers, the k_x^{-1} region does not exist (Ahn et al. 2013; Chin et al. 2014a); however, as the Reynolds number increases, the linear growth of energy between the inner and outer regions becomes active, and therefore, it is supposed that the active energy transfer helps to form the k_x^{-1} region.

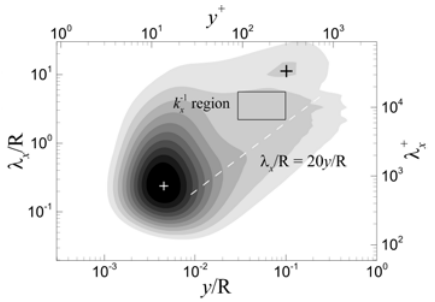

Figure 6: 2-D contour of the pre-multiplied streamwise energy spectra corresponding to the streamwise velocity fluctuations. The black solid box indicates the k_x^{-1} region (y^+ = 90 – 300 with λ_x/R = 2 – 5). The white dashed line indicates the linear growth of λ_x/R = 20y/R. The cross symbols represent the inner and outer sites at y^+ = 13 with λ_x^+ = 800 and y/R = 0.087 with λ_x/R = 10, respectively.

On the other hand, the energies of the VLSMs in the outer region are isolated from those of the SSMs and LSMs. As shown in figures 5, the energies of the VLSMs occurs at λ_x/R = 10 − 15 regardless of the wall-normal locations. This indicates that the VLSMs do not grow linearly with the wall-normal distance but exist with the fixed wavelengths; i.e., the VLSMs are not the attached eddies. In the energy sense, the SSMs and LSMs do not contribute to the formation of the VLSMs. Since the energy growth from the SSMs to LSMs becomes populated as increasing the Reynolds number, this energy transfer produces the large population of LSMs, and the generated adjacent LSMs result in the continuous concatenation along the streamwise direction, i.e., the VLSMs (Kim & Adrian 1999; Lee et al. 2014). In consequense, increasing the Reynolds number could produce the isolated energy peak of the VLSMs at long wavelengths. As the Reynolds number increases further, the energies associated with the VLSMs increase even more significantly. The deep valley shown in figures 5 and 6 would be filled with the large energies of the VLSMs at high Reynolds numbers.

CONCLUSIONS

A DNS of turbulent pipe flows is performed at a high Reynolds number, Re_τ = 3008. A long streamwise domain length of 30R is adopted to avoid the numerical artifact in high-order statistics. The streamwise mean velocity is found to follow the power law at y^+ = 90 – 300, as validated by the indicator function. The scale-separated Reynolds shear stress reveals that the presence of the constant-stress layer is more determined by the LSMs than the SSMs because the LSMs occupy more in the outer region than the SSMs. Because the LSMs are more populated in the channel flow than in the pipe flow, more active LSMs in the channel flow contribute to the constant-stress layer, continuing to the log law in the mean velocity, than they do in the pipe flow.The pre-multiplied streamwise spectra of the streamwise velocity fluctuations reveals the k_x^{-1} region for λ_x/R = 2 – 5 at the same wall-normal region of the power law. Linear growth of λ_x/R = 20y/R, from the small-scale to large-scale energies, develops the attached eddies, which form the k_x^{-1} region. The bimodal distribution with the spectral peaks of the LSMs and VLSMs is observed. The corresponding inner and outer site in the 2-D map of the energy spectra are located at y^+ = 13 with λ_x^+ = 800 and y/R = 0.087 with λ_x/R = 10.

ACKNOWLEDGEMENT

This work was supported by the Creative Research Initiatives (No. 2015-001828) program of the National Research Foundation of Korea (MSIP), and partially supported by the Supercomputing Center (KISTI).

REFERENCES

Ahn, J., Lee, J. H., Jang, S. J. and Sung, H. J., 2013, “Direct numerical simulations of fully developed turbulent pipe flows for Re_τ = 180, 544 and 934,” *Int. J. Heat Fluid Flow* Vol. 44, pp. 222-228.

Del Álamo, J. C and Jiménez, J., 2009, “Estimation of turbulent convection velocities and correlations to Taylor`s approximation,” *J. Fluid Mech.* Vol. 640, pp. 5-26.

Barenblatt, G. I., 1993, “Scaling laws for fully developed turbulent shear flows. Part 1. Basic hypotheses and analysis,” *J. Fluid Mech.* Vol. 248, pp. 513-520.

Chin, C., Hutchins, N., Ooi, A. and Marusic, I., 2011, “Spatial resolution correction for hot-wire anemometry in wall turbulence,” *Exp. Fluids* Vol. 50, pp. 1443-1453.

Chin, C., Monty, J. P. and Ooi, A., 2014a, “Reynolds number effects in DNS of pipe flow and comparison with channels and boundary layers,” *Int J. Heat Fluid Flow* Vol. 45, pp. 33–40.

Chin, C., Philip, J., Klewicki, J., Ooi, A. and Marusic, I., 2014b, “Reynolds-number-dependent turbulent inertia and onset of log region in pipe flows,” *J. Fluid Mech.* Vol. 757, pp. 747-769.

Hoyas, S. and Jiménez, J., 2006, “Scaling of the velocity fluctuations in turbulent channel up to Re_τ=2003,” *Phys. Fluids* Vol. 18, 011702.

Hultmark, M., Vallikivi, M., Bailey, S. C. C. and Smits, A. J., 2013, “Logarithmic scaling of turbulence in smooth- and rough-wall pipe flow,” *J. Fluid Mech.* Vol. 728, pp. 376–395.

Hutchins, N. and Marusic, I., 2007, "Evidence of very long meandering features in the logarithmic region of turbulent boundary layers," *J. Fluid Mech.* Vol. 579, pp. 1-28.

Kim, K. C. and Adrian, R. J., 1999, "Very large-scale motion in the outer layer," *Phys. Fluids* Vol. 11, pp. 417–422.

Kim, K., Baek, S. –J. and Sung, S. J., 2002, "An implicit velocity decoupling procedure for the incompressible Navier-Stokes equations," *Int. J. Numer. Method Fluids* Vol. 38, pp. 125–138.

Lee, J., Lee, J. H., Choi, J. -I., and Sung, H. J., 2014, "Spatial organization of large-and very-large-scale motions in a turbulent channel flow," *J. Fluid Mech.* Vol. 749, pp. 818-840.

Lee, J., Ahn, J. and Sung, H. J., 2015, "Comparison of large- and very-large-scale motions in turbulent pipe and channel flows," Phys. Fluids 27, 025101.

Marusic, I., Monty, J. P., Hultmark, M. and Smits, A. J., 2013, "On the logarithmic region in wall turbulence," *J. Fluid Mech.* Vol. 716, R3.

McKeon, B. J., Li, J., Jiang, W., Morrison, J. F. and Smit, A. J., 2004, "Further observations on the mean velocity distribution in fully developed pipe flow," *J. Fluid Mech.* Vol. 501, pp. 135–47.

Monty, J. P., Hutchins, N., Ng, H. C. H., Marusic, I. and Chong, M. S., 2009, "A comparison of turbulent pipe, channel and boundary layer flows," *J. Fluid Mech.* Vol. 632, pp. 431-442.

Morrison, J. F., Jiang, W., McKeon, B. J. and Smits, A. J., 2002, "Reynolds number dependence of streamwise velocity spectra in turbulent pipe flow," *Phys. Rev. Lett.* Vol. 88, 214501.

Nickels, T. B., Marusic, I., Hafez, S. and Chong, M. S., 2005, "Evidence of the k_1^{-1} law in a high-Reynolds-number turbulent boundary layer," *Phys. Rev. Lett.* Vol. 95, 074501.

Nickels, T. B., Marusic, I., Hafez, S., Hutchins, N. and Chong, M. S., 2007, "Some predictions of the attached eddy model for a high Reynolds number boundary layer," *Phil. Trans. R. Soc. A* Vol. 365, pp. 807–822.

Perry, A.E., Henbest, S. and Chong, M. S., 1986, "A theoretical and experimental study of wall turbulence," *J. Fluid Mech.* Vol. 165, pp. 163-199.

Rosenberg, B. J., Hultmark, M., Vallikivi, M., Bailey, S. C. C. and Smits, A. J., 2013, "Turbulence spectra in smooth- and rough-wall pipe flow at extreme Reynolds numbers," *J. Fluid Mech.* Vol. 731, pp. 46-63.

Townsend, A. A., 1976, "The Structure of Turbulent Shear Flow," *2nd edn*, Cambridge University Press.

Wu, X. and Moin, P., 2008, "A direct numerical simulation study on the mean velocity characteristics in turbulent pipe flow," *J. Fluid Mech.* Vol. 608, pp. 81-112.